

Photovoltaic performance of flexible perovskite solar cells under bending state

Daxue Du^{a,b}, Feiyang Qiao^b, Yikai Guo^a, Fengyan Wang^a, Linna Wang^a, Chao Gao^b, Dezhao Zhang^b, Jingjing Liang^b, Zhaopeng Xu^{c,*}, Wenzhong Shen^{b,d,*}, Haiyan Wang^{a,*}

^a State Key Laboratory of Metastable Materials Science and Technology, School of Environment and Chemical Engineering, Yanshan University, Qinhuangdao 066004, PR China

^b Institute of Solar Energy, and Key Laboratory of Artificial Structures and Quantum Control (Ministry of Education), School of Physics and Astronomy, Shanghai Jiao Tong University, Shanghai 200240, PR China

^c State Key Laboratory of Metastable Materials Science and Technology, School of Information Science and Engineering, Yanshan University, Qinhuangdao 066004, PR China

^d Collaborative Innovation Center of Advanced Microstructures, Nanjing 210093, PR China

ARTICLE INFO

Keywords:

Flexible perovskite solar cells
Bending state
Angles and directions
Mechanical and optical
Silica subwavelength array

ABSTRACT

Although flexible perovskite solar cells have made extensive progress, there is a lack of investigation on the performance of flexible perovskite solar cells under bending state. Here, two-dimensional models of flexible perovskite solar cells have been performed to reveal the effect of bending angles and directions for the first time. Simulated results are in good agreement with experimentally reported data, validating the accuracy of our model. To optimize mechanical and optical performance under bending state, silica subwavelength array is embedded on the surface of the flexible substrate. Hence, the current density of flexible perovskite solar cells has been improved by 7.3% at downwards bending 60° and 1.9% at upwards bending 60°. Our work provides a guide for the design of efficient flexible perovskite solar cells under bending state.

1. Introduction

With the vigorous development of perovskite devices, flexible perovskite solar cells have attracted an increasing number of attentions (Bae et al., 2022; Hu et al., 2021; Green et al., 2022; Min et al., 2021). Traditional perovskite devices are prepared on the bulky and fragile glass substrates, which limits their application in the fields of building integrated photovoltaics, wearable devices, space energy, etc (Batumunkh et al., 2020; Huang et al., 2020; Lang et al., 2016; Yin et al., 2016; Yoon et al., 2017). These application requirements can be met by fabricating perovskite solar cells on a flexible substrate because of the excellent quality of lightness, portability, and flexibility (Yoon et al., 2017), which are available for the flexible perovskite solar cell (FPSC) including polymers, metal foils, carton materials, and flexible glass (Babu et al., 2020; Dong et al., 2017; Dou et al., 2017; Jin et al., 2021; Roldán-Carmona et al., 2014). Although the first FPSC was fabricated with a power conversion efficiency (η) of 2.62% (Kumar et al., 2013), the η of FPSC has made great progress to reach 21.75% so far (Cao et al.,

2019; Meng et al., 2020; Wu et al., 2021) with the development of functional materials and low-temperature manufacturing technologies.

For FPSC, the bending performance is extremely vital because FPSC needs to work with a bending state in using scenarios (Yang et al., 2019). Most research on the bending performance of FPSC has been carried out to evaluate the performance after thousands of mechanical bends but ignore the performance under bending state (Chang et al., 2015; Chen et al., 2020; Jiang et al., 2021; Park et al., 2017; Wang et al., 2017; Xiong et al., 2018). Fortunately, this situation has improved in recent studies. Kim et al. carried out the research on the mechanical bending performance of FPSC under different curvature radii for the first time (Kim et al., 2015). Even if the bending radius is as low as 1 mm, the η does not be significantly reduced, reaching 93% of the original value. In 2018, Shengzhong Liu group (Feng et al., 2018) provided a similar result. The η is reduced by 17% when the curvature radius is as small as 4 mm. Recently, Wu et al. (Wu et al., 2021) achieved a champion efficiency of 21.73% in FPSC to date, and they also measured the η to 94% of the initial value at a curvature radius of 4 mm. Due to the limitations of the

* Corresponding authors at: Institute of Solar Energy, and Key Laboratory of Artificial Structures and Quantum Control (Ministry of Education), School of Physics and Astronomy, Shanghai Jiao Tong University, Shanghai 200240, PR China (W. Shen).

E-mail addresses: xuzhaopeng1@163.com (Z. Xu), wzshen@sjtu.edu.cn (W. Shen), hywang@ysu.edu.cn (H. Wang).

test equipment, although it has been demonstrated that the degree of bending has little effect on the η of well-prepared devices, no one has studied the effect of bending on the light absorption inside the device in detail, so the photovoltaic performance slightly improved at a small bending angle has not been appreciated and analyzed in previous reports (Hu et al., 2019; Wang et al., 2020; Zhao et al., 2020). Furthermore, there is also a lack of research on the effect of bending direction on the photovoltaic performance of FPSC.

Hence, we report a solution to calculate the surface stress and photovoltaic performance of FPSC under different bending angles and directions based on Comsol Multiphysics software. Our results verify the experimental reports, the η still maintains 95.12 % of the initial value in FPSC when bent to 90°. However, the bending direction generates a huge difference in photovoltaic performance. Bending up is 9.9 % higher than bending down in current density. Moreover, in order to further improve the working performance at a bent state, silica nanospheres are introduced and embedded on the surface of the FPSC (Das et al., 2019; Du et al., 2021a; Yoo et al., 2020). After the introduction of silica nanospheres as the light-trapping structure, the η of FPSC has raised, reaching 19.72 % increased by 7.3 % at downwards bending 60°, and 20.26 % increased by 1.9 % at upwards bending 60°. And the mechanical properties of the FPSC in the bent state are also improved.

2. Simulated and experimental methods

The two-dimensional simulations of photovoltaic performance under different bending angles are studied by Comsol Multiphysics software (Wave Optics Module). The schematics of FPSC are shown in Fig. 1, which is constructed on Polydimethylsiloxane flexible substrate (PDMS, 2 μm), followed by Indium tin oxide (ITO, 100 nm) as the transparent electrode, TiO_2 (60 nm) as the electron transport layer, MAPbI_3 (500 nm) as the perovskite active layer, SpiroOMeTAD (150 nm) as the hole transport layer, and Au film (100 nm). The types and thicknesses of materials for FPSC are consistent with our experimental work, except that the PDMS substrate was set as 2 μm to reduce the simulation time. The standard AM 1.5G spectrum is introduced as the incident light source, and the refractive indexes and extinction coefficients of the stacks of FPSCs are taken from pieces of literature (Wu et al., 2016; Du et al., 2021b), as shown in Fig. S1. The fabrication methods and characterization data (SEM, XRD, PL, and J-V curves) of the device are placed in supporting information. Furthermore, to investigate the mechanical failure mechanism of FPSC upon bending, finite element mechanical modeling was carried out using Comsol Multiphysics software (Solid Mechanics Module). The material parameters (Tavakoli et al., 2016) used in the model are listed in Table S1.

3. Results and discussion

As shown in Fig. 2a, a flexible device is simply considered to be bent

symmetrically, so the calculation amount can be reduced by half. With L_0 set as 10 μm , the illuminated length (L) and corresponding curvature radius (R) resulting from the change of the bending angle (θ) are listed in Table S2. Fig. 2b displays the measured and simulated reflectance spectra of the horizontal flexible solar cells. The simulated reflectance spectra are generally in agreement with the measured results, which lays a good foundation for research on the performance in the bending state. Noted that in order to simplify the calculation, the thickness of the PDMS substrate was set much smaller than the actual value producing resonance effect (Haider et al., 2011). The reflectance of the bending FPSCs compared with the planar one is generally reduced, as drawn in Fig. 2b–c. With the bending angle increasing, the vibration intensity of the reflectance spectra gradually weakens. Moreover, the variation of the reflectance spectra with bending angles exhibits wavelength-dependent characteristics. We provided the average reflectance of the typical waveband 450–550 nm and 650–750 nm in Fig. 2d, where the changes in the reflectance spectra are quite different. In general, the average reflectance first decreased and then increased during 450–550 nm reaching the minimum value around 45° with bending angles increasing, but the reflectance gradually increased during 650–750 nm.

In order to further explore the difference of FPSCs based on bending angles, the electric field distribution at the wavelength of 550 nm was plotted in Fig. 3. It can be observed that the electric field of a horizontal FPSC exhibits a uniform fringe shape, while the electric field of the downwards bending FPSCs exhibits arc shape and converges towards the center. In particular, as the degree of bending deepens, the electric field intensity inside FPSCs gradually increases due to the light centripetal convergence of the bending surface, which leads to a 1.7 times improvement in the maximum electric field inside FPSC bent at 90° compared to 0°. Additionally, the electric field intensity at the edge of the FPSC is very weak certifying that the incident light cannot reach this region. With the deepening of the bending angle, the weak electric field region near the bending center of the FPSC gradually disappears, while gradually expanding near the edge region, because the light is further concentrated in the centripetal owing to the reduced curvature radius.

Thereafter, the carrier generation rate can be further obtained from the electric field intensity according to equation (1) to visualize the electrical properties under different bending angles.

$$g(\lambda) = \frac{\epsilon''(\lambda)|E(\lambda)|^2}{2\hbar} \quad (1)$$

Where $\epsilon''(\lambda)$ is the extinction coefficient of material drawn in Fig. S1, $E(\lambda)$ is the electric field intensity, and \hbar is the reduced Planck constant. As exhibited in Fig. 4, the carrier generation rate in the perovskite active layer is much higher than that in other regions, except for the Ag surface in the horizontal condition due to a very large extinction coefficient of Ag. As the degree of bending deepens, the incident light is further concentrated near the bending center and difficult to reach the edge, causing the magnitude of the carrier generation rate decreases from the

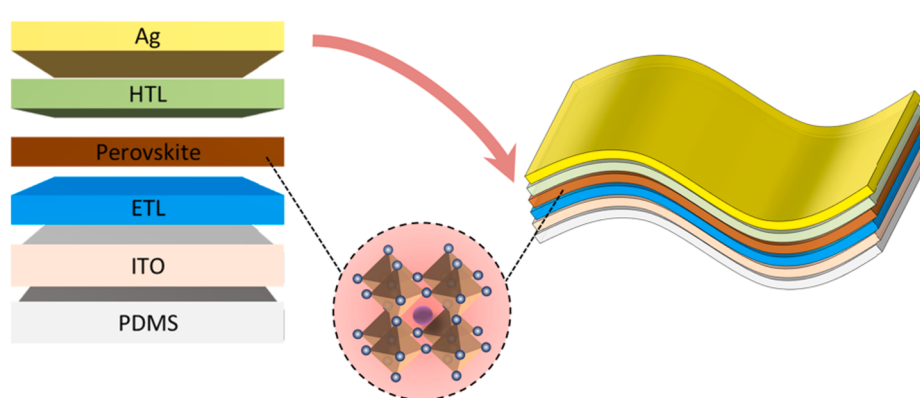


Fig. 1. The schematics of the flexible perovskite solar cells.

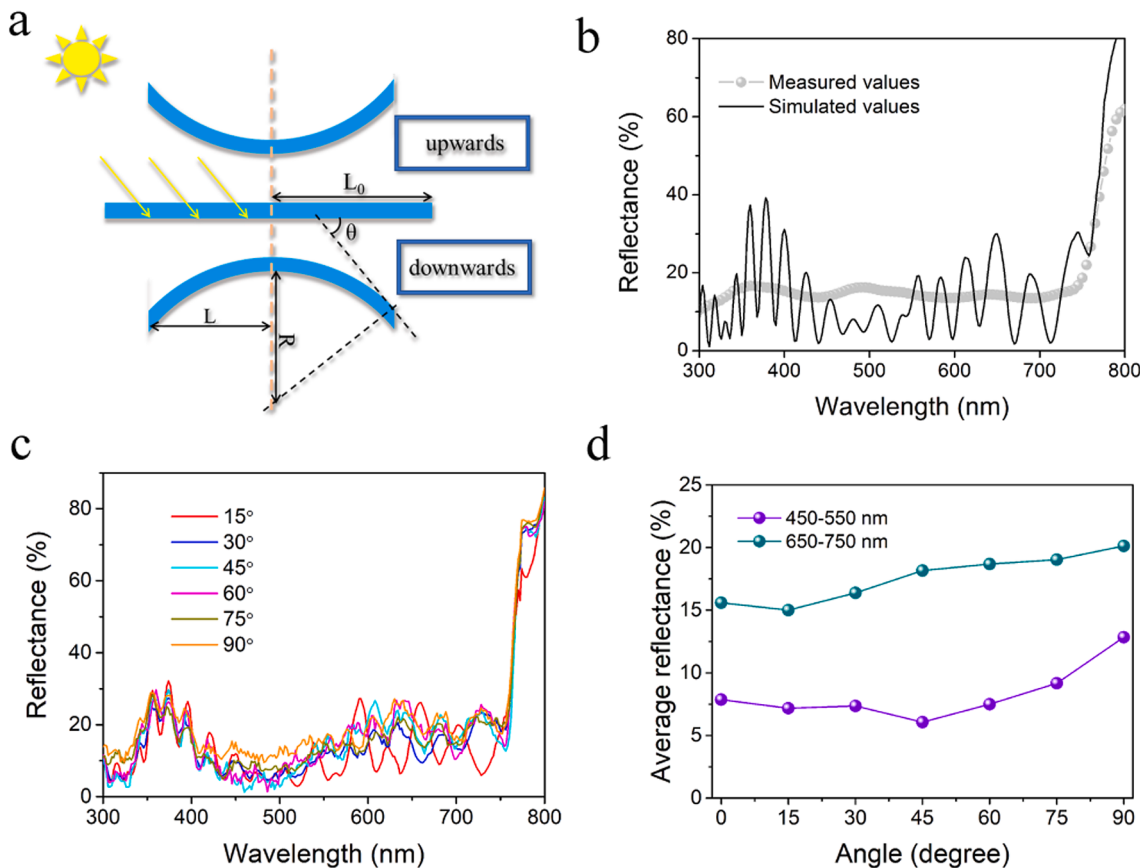


Fig. 2. (a) Schematic diagram of the geometric relationship of the FPSC under bending state, (b) Measured and simulated reflectance spectra of horizontal FPSC (0°), (c) Reflectance spectra of FPSCs at different bending angles, (d) The average reflectance of FPSCs during 450–550 nm and 650–750 nm at different bending angles.

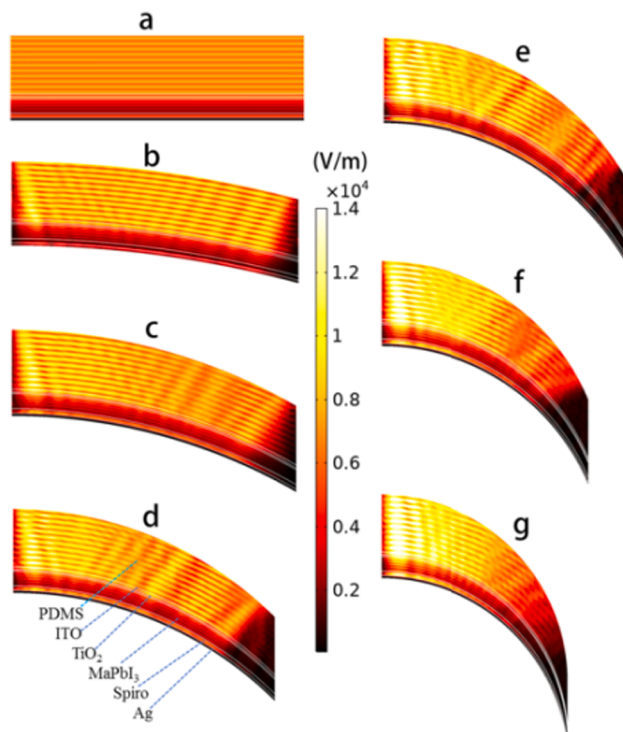


Fig. 3. The electric field distribution of FPSCs at different bending angles, (a) 0° , (b) 15° , (c) 30° , (d) 45° , (e) 60° , (d) 75° , (e) 90° .

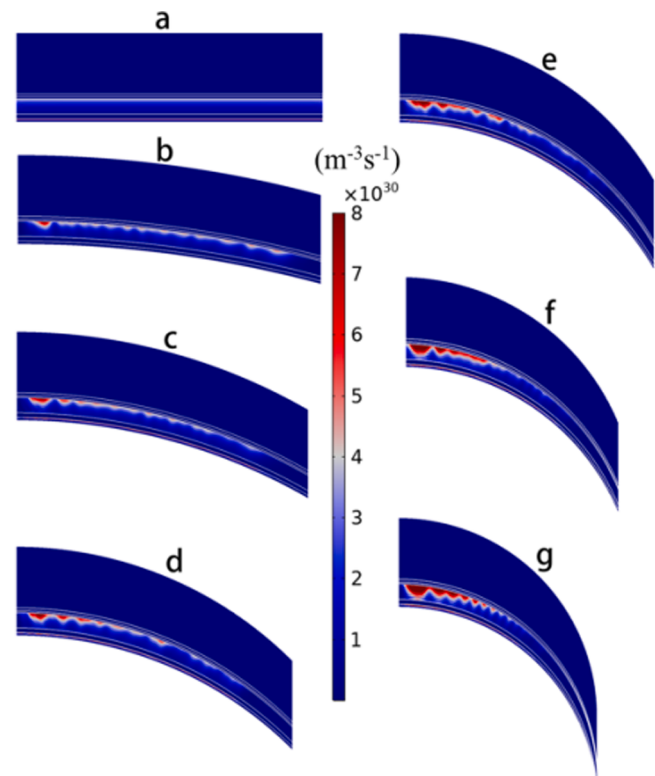


Fig. 4. The carrier generation rate (g) of FPSCs at different bending angles, (a) 0° , (b) 15° , (c) 30° , (d) 45° , (e) 60° , (d) 75° , (e) 90° .

bending center to the edge. The maximum carrier generation rate of the downwards bending perovskite layer occurs on the surface around the bending center, in order of $0.45 (\times 10^{31} \text{ m}^{-3} \text{s}^{-1})$ for 0° , followed by 0.87 for 15° , 5.56 for 30° , 7.00 for 45° , 8.39 for 60° , 10.11 for 75° , and 12.62 for 90° .

Fig. 5(a-c) reveal the corresponding absorption spectra of FPSC under downwards bending 0° , 45° and 90° . The horizontal perovskite active layer has weak light absorption due to strongly parasitic absorption by the ITO and TiO_2 layers below the wavelength of 360 nm in Fig. 5a. With the increasing wavelength, the absorbance of ITO and TiO_2 decreases rapidly. In the wavelength range from 360 to 750 nm , the light is absorbed by MaPbI_3 to generate photocurrent, and MaPbI_3 produces strong radiation loss around 750 nm demonstrated by the photoluminescence spectrum of Fig. S3. As the bending angle increases, there is a slight decrease in parasitic absorption of ITO and TiO_2 , but the effect of this change on the current density is almost negligible. Therefore, the evaluation about the effect of bending angle can be simplified by comparing the external quantum efficiency (EQE) of FPSC. Fig. 5d shows the EQE of FPSC under bending angles from 0° to 90° , clearly presenting the wavelength-dependent characteristics, which are in good agreement with the reflectance spectra in Fig. 2c.

Based on the standard solar spectra and the EQE spectra, J_{SC} varying with bending angles can be calculated using equation (2).

$$J_{SC} = \frac{q}{hc} \int_{300 \text{ nm}}^{800 \text{ nm}} \lambda \text{EQE}(\lambda) \phi_{AM\ 1.5G}(\lambda) d\lambda \quad (2)$$

Where q is the electron charge, $\phi_{AM\ 1.5G}(\lambda)$ is the standard solar spectra AM 1.5G. The corresponding current densities of reflection and EQE under different downwards bending angles are shown in Fig. 5e. Remarkably, the current density of FPSC increases slightly from 21.78 mA/cm^2 to 22.29 mA/cm^2 during mild bending, which is consistent with the results reported in many works (Hu et al., 2019; Wang et al., 2020; Zhao et al., 2020). Because the bending leads to an increase in the thickness of the absorber layer, and the absorption is improved. However, as the angle increases above 15° , the current density gradually decreases, owing to the thickness of the absorbing layer being large enough to almost reach saturated absorption (Qarony et al., 2020; Zheng

and Xuan, 2021). It does not significantly improve the absorption but leads to an increase in reflection for continuing to bend, so antagonism between the two results in a further reduction in absorption. Bending not only affects the absorption of the FPSC but also seriously reduces the illuminated area, which has to be considered in the energy yield. Considering the effect of bending on L , the ratio of bending 90° to 0° is 0.953 of current density but of 0.607 the current. Fig. 5f clearly presents that $J-V$ curves of FPSCs at different bending angles have small changes in η compared to 18.65% of the flat one (0°), which are 19.11% for 15° , 18.74% for 30° , 18.47% for 45° , 18.32% for 60° , 18.11% for 75° , 17.74% for 90° , with key parameters summarized in Table S3. The η of the FPSC remains at 95.12% of the initial value (0°), even when the device is bent to 90° . The measured η of horizontal FPSC is 14.26% drawn in Fig. S2d. As a comparison, we used ideal parallel and series resistors under simulated conditions, resulting in higher simulated results than measured values.

Interestingly, the bending direction of FPSC has a huge impact on the optical performance. The farther away from the bending center, the electric field intensity of the upward bending FPSC is larger taking the bending 60° as examples shown in Fig. 6, which is completely opposite to that of the downward bending. More importantly, there is almost no region that light cannot be absorbed under the upward bending, which will significantly improve the absorption compared to downwards bending as shown in Fig. 6a. Hence, FPSC upwards bending 60° has a current density as high as 23.54 mA/cm^2 , obtaining 2.13 mA/cm^2 higher than downwards 60° , which is mainly due to the large increase in absorption in the waveband during 650 – 750 nm as evidenced by the absorption curves in Fig. 6b.

To improve mechanical and optical performance under bending state, we use silica subwavelength array (SSA) for FPSC as the light trapping structure with a diameter of 600 nm and a pitch of 700 nm (Grandidier et al., 2011; Mihi et al., 2013). Firstly, the stress distributions of bending FPSCs based on PDMS and several different PDMS@SiO₂ substrates were calculated in Fig. 7, because the stress distribution of FPSC has a great influence on the flexibility. The high surface stress is mainly concentrated on the ITO, TiO_2 and Ag layers near the bent center due to their great elastic modulus and Poisson's ratios, and the maximum stress is concentrated at Ag layer owing to the stress

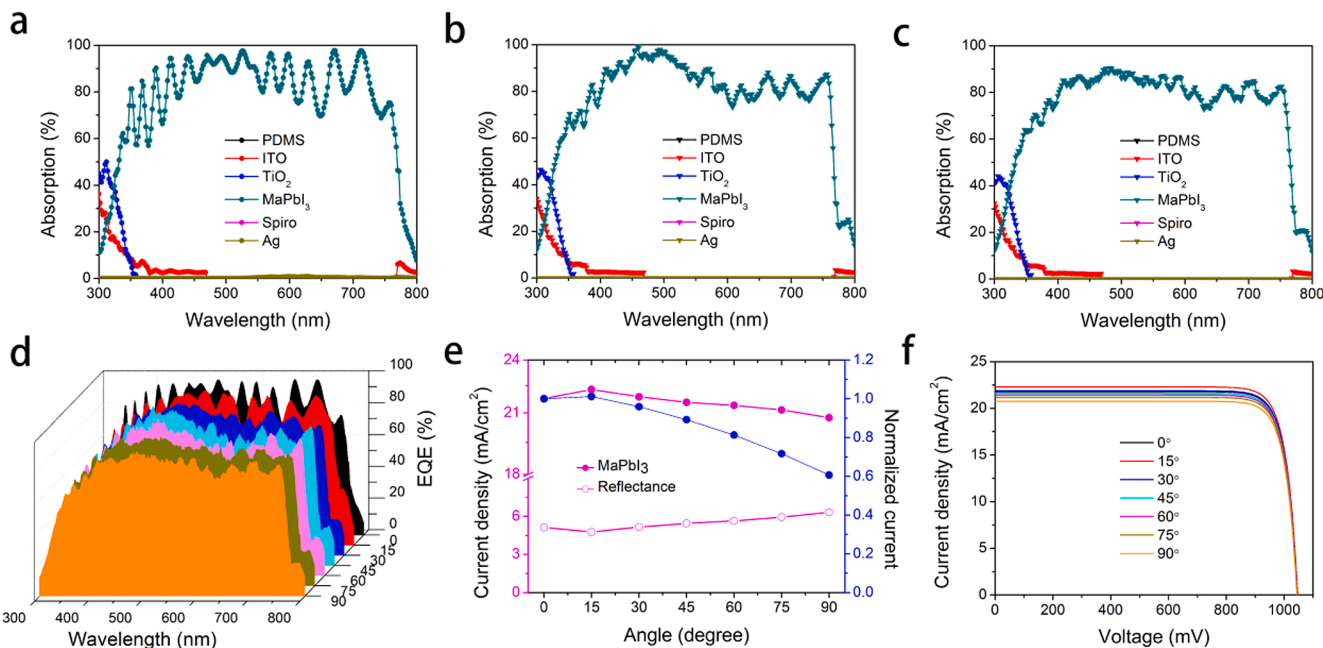


Fig. 5. Absorption spectra of each absorbing layer of FPSCs at downwards bending (a) 0° , (b) 45° , and (c) 90° , (d) EQE of FPSCs with different downwards bending angles, (e) Current density and normalized current of FPSCs with different downwards bending angles, (f) $J-V$ curves of FPSCs at different downwards bending angles.

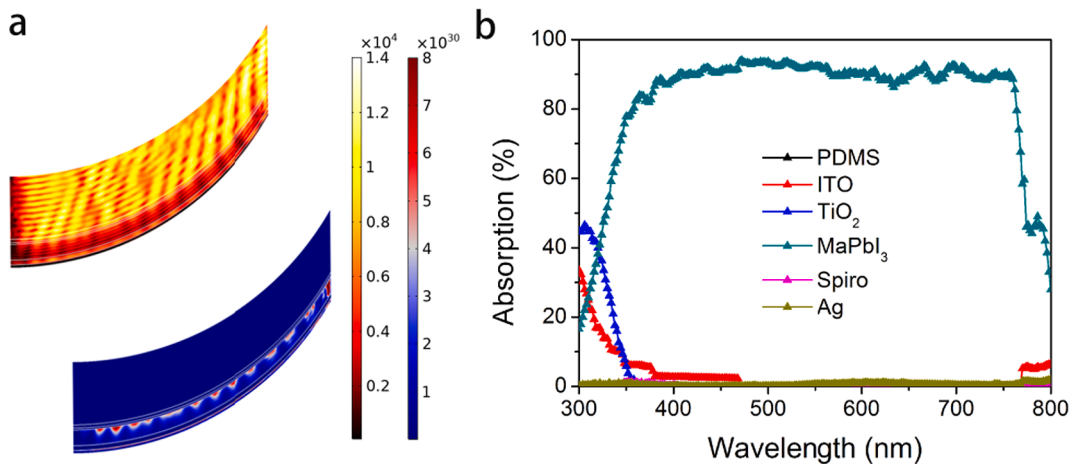


Fig. 6. (a) The electric field distribution and carrier generation rate of FPSCs at upwards bending 60°, (b) Absorption spectra of each absorbing layer of FPSCs at upwards bending 60°.

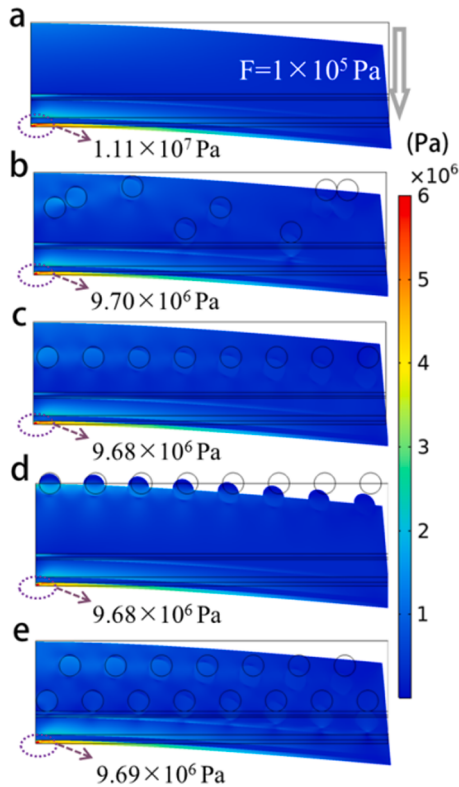


Fig. 7. Stress distributions of FPSCs based on (a) PDMS and (b)-(e) PDMS@SiO₂ substrates.

transmitted to the bottom layer. The introduction of SiO₂ nanospheres effectively reduces the bending stress of the FPSC from 1.11×10^7 Pa to 9.68×10^6 Pa, and this reduction effect is basically independent of the distribution of SiO₂ nanospheres. This demonstrates the gain in device flexibility with the introduction of SSA. Moreover, we verified a small effect of different diameters and pitches of silica nanospheres on the stress distribution placed on Fig. S3.

Secondly, the introduction of SSA on the surface of FPSC provides excellent light trapping, which can be observed by the prominent electric field peaks under silica nanosphere at bending 60° in Fig. 8(a-b), because the SSA on the surface of FPSC can produce whispering gallery modes, forming the high electric field intensity until poured into the perovskite absorption layer (Grandidier et al., 2011). In contrast, no

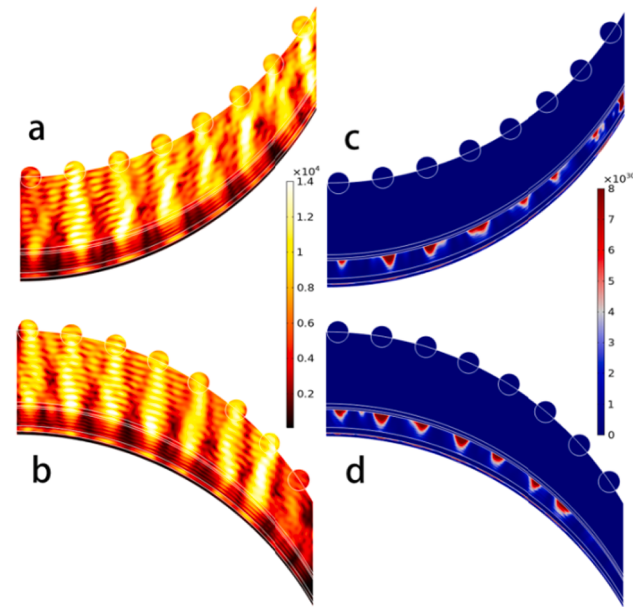


Fig. 8. The electric field distribution (a-b) and carrier generation rate (c-d) of FPSCs with SSA at different bending directions.

strong electric field peaks can be observed when the silica nanospheres are located inside PDMS film, which is displayed in Fig. S4-S7. In addition, the electric field strength in the bent center gradually decays to the edge under upwards bending, while the opposite is true for the downwards bending. Benefiting from the excellent light trapping effect of SSA, the magnitude and depth of the carrier generation rate inside FPSC are greatly improved, which can be clearly observed in Fig. 8(c-d).

Similarly, the absorption of FPSCs with SSA was explored at different directions as shown in Fig. 9(a-b). The active layer of the FPSC upwards bending is significantly enhanced compared to downwards bending device, especially in the 550–750 nm. Owing to the upwards bending surface of FPSC being condensed, so the reflectance is low. On the contrary, the reflectance is high for a downwards bending surface of FPSC. The introduction of silica nanospheres as light trapping structure on the surface of FPSC significantly improves the light absorption between downward bending and upward bending because of the decreased reflectance in broad spectral ranges. As exhibited in Fig. 8c, the bare FPSCs exhibit J_{sc} of 21.41 mA/cm² and η of 18.32 % at downwards bending 60°; J_{sc} of 23.54 mA/cm² and η of 20.23 % at upwards bending

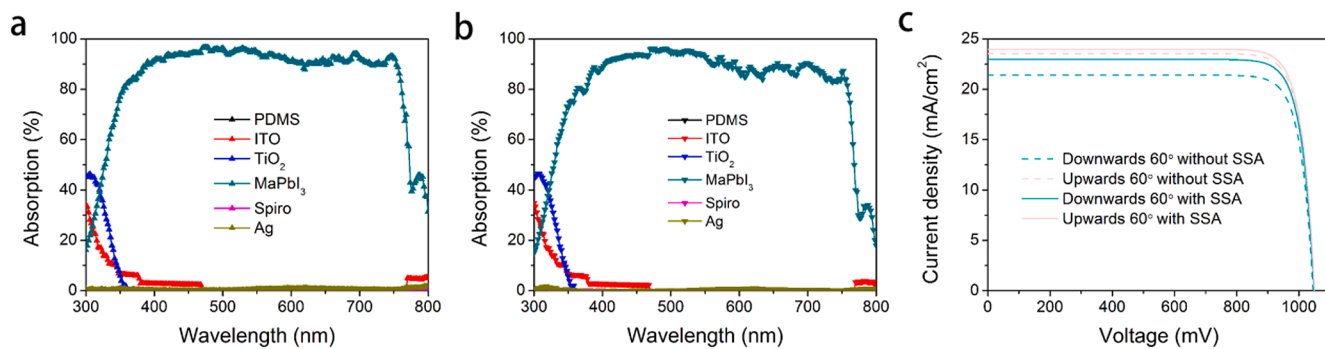


Fig. 9. Absorption spectra of each absorbing layer of FPSCs with SSA at bending (a) upwards 60° and (b) downwards 60°, (c) J-V curves of FPSCs without and with SSA at bending 60°.

60°. With introducing SSA as light-trapping nanostructures, the η of FPSCs with SSA is increased to 19.72 % (down 60°) and 20.26 % (up 60°), which is attributed to an increase of 7.3 % and 1.9 % in J_{sc} . The detailed parameters are listed in Table S3. Obviously, the effect of introducing SSA is more pronounced, when FPSC is bent downwards because of an outstanding light converging effect, achieving a high current density of 23.54 mA/cm² at bending upwards 60°.

4. Conclusion

In conclusion, the simulations of the different bent angles and directions on the photovoltaic performance are carefully investigated based on the data of our fabricated FPSC. The absorption of FPSCs is slightly improved under bending 15°, but begins to decrease under bending over 15°, which is mainly due to the antagonistic effect of the reflectance loss and the increase of active layer thickness in the bent state. And bending up has much less reflection loss than bending down due to light converging. Silica nanospheres are introduced into the surface and interior of the flexible substrate in order to further improve the performance under bending working conditions. When silica nanospheres are embedded on the surface of PDMS film, the η of the FPSC respectively reaches to 19.72 % and 20.62 % at bending 60° down and up, respectively. In addition, the introduction of SSA reduces stress on metal electrodes in the bending state of FPSC through the comparison of surface stress distribution. The simulation results would offer the insight of the performance of FPSCs under bent working conditions, and be useful for further application and design optimization of device.

Declaration of Competing Interest

The authors declare that they have no known competing financial interests or personal relationships that could have appeared to influence the work reported in this paper.

Acknowledgments

This work was supported by the National Natural Science Foundation of China (No. 11834011), Training Programme Fund for Talents of Hebei Province (A201902010), Fund of Science and Technology Project of Hebei Education Department (QN2020122). The simulations in this paper have been done on the supercomputing system in the Computing Center of Yanshan University.

Appendix A. Supplementary data

Supplementary data to this article can be found online at <https://doi.org/10.1016/j.solener.2022.08.070>.

References

- Babu, V., Fuentes Pineda, R., Ahmad, T., Alvarez, A.O., Castriotta, L.A., Di Carlo, A., Fabregat-Santiago, F., Wojciechowski, K., 2020. Improved Stability of Inverted and Flexible Perovskite Solar Cells with Carbon Electrode. *ACS Appl. Energy Mater.* 3 (6), 5126–5134.
- Bae, S., Noh, Y.W., Park, D.-S., Song, M.H., Choi, S.-W., 2022. Development of colored perovskite solar cells using cholesteric helicoidal superstructures. *Nano Energy* 93, 106801.
- Batmunkh, M., Zhong, Y.L., Zhao, H., 2020. Recent Advances in Perovskite-Based Building-Integrated Photovoltaics. *Adv. Mater.* 32 (31), 2000631.
- Cao, B., Yang, L., Jiang, S., Lin, H., Wang, N., Li, X., 2019. Flexible quintuple cation perovskite solar cells with high efficiency. *J. Mater. Chem. A* 7 (9), 4960–4970.
- Chang, C.-Y., Chu, C.-Y., Huang, Y.-C., Huang, C.-W., Chang, S.-Y., Chen, C.-A., Chao, C.-Y., Su, W.-F., 2015. Tuning Perovskite Morphology by Polymer Additive for High Efficiency Solar Cell. *ACS Appl. Mater. Interfaces* 7 (8), 4955–4961.
- Chen, H., Wang, H., Wu, J., Wang, F., Zhang, T., Wang, Y., Liu, D., Li, S., Penty, R.V., White, I.H., 2020. Flexible optoelectronic devices based on metal halide perovskites. *Nano Research* 13 (8), 1997–2018.
- Das, S., Hossain, M.J., Leung, S.-F., Lenox, A., Jung, Y., Davis, K., He, J.-H., Roy, T., 2019. A leaf-inspired photon management scheme using optically tuned bilayer nanoparticles for ultra-thin and highly efficient photovoltaic devices. *Nano Energy* 58, 47–56.
- Dong, Q., Shi, Y., Zhang, C., Wu, Y., Wang, L., 2017. Energetically favored formation of SnO₂ nanocrystals as electron transfer layer in perovskite solar cells with high efficiency exceeding 19%. *Nano Energy* 40, 336–344.
- Dou, B., Miller, E.M., Christians, J.A., Sanehira, E.M., Klein, T.R., Barnes, F.S., Shaheen, S.E., Garner, S.M., Ghosh, S., Mallick, A., Basak, D., van Hest, M.F.A.M., 2017. High-Performance Flexible Perovskite Solar Cells on Ultrathin Glass: Implications of the TCO. *J. Phys. Chem. Lett.* 8 (19), 4960–4966.
- Du, D., Zeng, Y., Wang, C., Li, M., Wang, F., Xu, Z., Wang, H., 2021a. Broadband antireflection enhancement of c-Si solar cells by less 1/10 wavelength and subwavelength of silica nanosphere coatings. *Opt. Mater.* 114, 110957.
- Du, D., Xu, Z., Wang, L., Guo, Y., Liu, S., Yu, T., Wang, C., Wang, F., Wang, H., 2021b. The broadband and omnidirectional antireflective performance of perovskite solar cells with curved nanostructures. *Sol. Energy* 224, 10–17.
- Feng, J., Zhu, X., Yang, Z., Zhang, X., Niu, J., Wang, Z., Zuo, S., Priya, S., Liu, S., Yang, D., 2018. Record Efficiency Stable Flexible Perovskite Solar Cell Using Effective Additive Assistant Strategy. *Adv. Mater.* 30 (35), 1801418.
- Grandidier, J., Callahan, D.M., Munday, J.N., Atwater, H.A., 2011. Light Absorption Enhancement in Thin-Film Solar Cells Using Whispering Gallery Modes in Dielectric Nanospheres. *Adv. Mater.* 23 (10), 1272–1276.
- Green, M.A., Dunlop, E.D., Hohl-Ebinger, J., Yoshita, M., Kopidakis, N., Hao, X., 2022. Solar cell efficiency tables (version 9.0). *Prog. Photovoltaics* 30 (1), 3–12.
- Haider Butt, Q.D., Rajasekharan, R., Wilkinson, T.D., Amarasinghe, G.A.J., 2011. Enhanced reflection from arrays of silicon based inverted nanocones. *Appl. Phys. Lett.* 99, 133105.
- Hu, X., Meng, X., Zhang, L., Zhang, Y., Cai, Z., Huang, Z., Su, M., Wang, Y., Li, M., Li, F., Yao, X., Wang, F., Ma, W., Chen, Y., Song, Y., 2019. A Mechanically Robust Conducting Polymer Network Electrode for Efficient Flexible Perovskite Solar Cells. *Joule* 3 (9), 2205–2218.
- Hu, Y., Niu, T., Liu, Y., Zhou, Y., Xia, Y., Ran, C., Wu, Z., Song, L., Müller-Buschbaum, P., Chen, Y., Huang, W., 2021. Flexible Perovskite Solar Cells with High Power-Per-Weight: Progress, Application, and Perspectives. *ACS Energy Lett.* 6 (8), 2917–2943.
- Huang, K., Yang, K., Li, H., Zheng, S., Wang, J., Guo, H., Peng, Y., Zhong, X., Yang, J., 2020. γ -ray Radiation on Flexible Perovskite Solar Cells. *ACS Appl. Energy Mater.* 3 (8), 7318–7324.
- Jiang, N.-R., Wang, Y.-F., Dong, Q.-F., Ge, C.-D., Yang, Z.-Q., Yin, D., Liu, Y.-F., Bi, Y.-G., Feng, J., Sun, H.-B., 2021. Enhanced Efficiency and Mechanical Robustness of Flexible Perovskite Solar Cells by Using HPbI₃ Additive. *Sol. RRL* 5 (4), 2000821.
- Jin, JunJun, Li, J., Tai, Q., Chen, Y., Mishra, D.D., Deng, W., Xin, J., Guo, S., Xiao, B., Wang, X., 2021. Efficient and stable flexible perovskite solar cells based on graphene-AgNWs substrate and carbon electrode without hole transport materials. *J. Power Sources* 482, 228953.

- Kim, B.J., Kim, D.H., Lee, Y.-Y., Shin, H.-W., Han, G.S., Hong, J.S., Mahmood, K., Ahn, T.K., Joo, Y.-C., Hong, K.S., Park, N.-G., Lee, S., Jung, H.S., 2015. Highly efficient and durable perovskite solar cells: toward a wearable power source. *Energy Environ. Sci.* 8 (3), 916–921.
- Kumar, M.H., Yantara, N., Dharani, S., Graetzel, M., Mhaisalkar, S., Boix, P.P., Mathews, N., 2013. Flexible, low-temperature, solution processed ZnO-based perovskite solid state solar cells. *Chem. Commun.* 49 (94), 11089.
- Lang, F., Nickel, N.H., Bundesmann, J., Seidel, S., Denker, A., Albrecht, S., Brus, V.V., Rappich, J., Rech, B., Landi, G., Neitzert, H.C., 2016. Radiation Hardness and Self-Healing of Perovskite Solar Cells. *Adv. Mater.* 28 (39), 8726–8731.
- Meng, X., Cai, Z., Zhang, Y., Hu, X., Xing, Z., Huang, Z., Huang, Z., Cui, Y., Hu, T., Su, M., Liao, X., Zhang, L., Wang, F., Song, Y., Chen, Y., 2020. Bio-inspired vertebral design for scalable and flexible perovskite solar cells. *Nat. Commun.* 11 (1), 3016.
- Mihi, A., Bernechea, M., Kufer, D., Konstantatos, G., 2013. Coupling Resonant Modes of Embedded Dielectric Microspheres in Solution-Processed Solar Cells. *Adv. Opt. Mater.* 1 (2), 139–143.
- Min, H., Lee, D.Y., Kim, J., Kim, G., Lee, K.S., Kim, J., Paik, M.J., Kim, Y.K., Kim, K.S., Kim, M.G., Shin, T.J., Il Seok, S., 2021. Perovskite solar cells with atomically coherent interlayers on SnO₂ electrodes. *Nature* 598 (7881), 444–450.
- Park, J.-I., Heo, J.H., Park, S.-H., Hong, K.I., Jeong, H.G., Im, S.H., Kim, H.-K., 2017. Highly flexible InSnO electrodes on thin colourless polyimide substrate for high-performance flexible CH₃NH₃PbI₃ perovskite solar cells. *J. Power Sources* 341, 340–347.
- Qarony, W., Hossain, M.I., Jovanov, V., Salleo, A., Knipp, D., Tsang, Y.H., 2020. Influence of Perovskite Interface Morphology on the Photon Management in Perovskite/Silicon Tandem Solar Cells. *ACS Appl. Mater. Interfaces* 12 (13), 15080–15086.
- Roldán-Carmona, C., Malinkiewicz, O., Soriano, A., Mínguez Espallargas, G., García, A., Reinecke, P., Kroyer, T., Dar, M.I., Nazeeruddin, M.K., Bolink, H.J., 2014. Flexible high efficiency perovskite solar cells. *Energy Environ. Sci.* 7 (3), 994.
- Tavakoli, M.M., Lin, Q., Leung, S.F., Lui, G.C., Lu, H., Li, L., Xiang, B., Fan, Z., 2016. Efficient, flexible and mechanically robust perovskite solar cells on inverted nancone plastic substrates. *Nanoscale* 8 (7), 4276–4283.
- Wang, C., Guan, L., Zhao, D., Yu, Y., Grice, C.R., Song, Z., Awani, R.A., Chen, J., Wang, J., Zhao, X., Yan, Y., 2017. Water Vapor Treatment of Low-Temperature Deposited SnO₂ Electron Selective Layers for Efficient Flexible Perovskite Solar Cells. *ACS Energy Lett.* 2 (9), 2118–2124.
- Wang, Z., Zeng, L., Zhang, C., Lu, Y., Qiu, S., Wang, C., Liu, C., Pan, L., Wu, S., Hu, J., Liang, G., Fan, P., Egelhaaf, H.J., Brabec, C.J., Guo, F., Mai, Y., 2020. Rational Interface Design and Morphology Control for Blade-Coating Efficient Flexible Perovskite Solar Cells with a Record Fill Factor of 81%. *Adv. Funct. Mater.* 30 (32), 2001240.
- Wu, S., Li, Z., Zhang, J., Wu, X., Deng, X., Liu, Y., Zhou, J., Zhi, C., Yu, X., Choy, W.C.H., Zhu, Z., Jen, A.K.Y., 2021. Low-Bandgap Organic Bulk-Heterojunction Enabled Efficient and Flexible Perovskite Solar Cells. *Adv. Mater.* 33 (51), 2105539.
- Wu, X., Liu, P., Ma, L., Zhou, Q., Chen, Y., Lu, J., Yang, S.E., 2016. Two-dimensional modeling of TiO₂ nanowire based organic-inorganic hybrid perovskite solar cells. *Sol. Energy Mater. Sol. Cells* 152, 111–117.
- Xiong, H., DeLuca, G., Rui, Y., Zhang, B., Li, Y., Zhang, Q., Wang, H., Reichmanis, E., 2018. Modifying Perovskite Films with Polyvinylpyrrolidone for Ambient-Air-Stable Highly Bendable Solar Cells. *ACS Appl. Mater. Interfaces* 10 (41), 35385–35394.
- Yang, D., Yang, R., Priya, S., Liu, S., 2019. Recent Advances in Flexible Perovskite Solar Cells: Fabrication and Applications. *Angew. Chem. Int. Ed.* 58 (14), 4466–4483.
- Yin, X., Chen, P., Que, M., Xing, Y., Que, W., Niu, C., Shao, J., 2016. Highly Efficient Flexible Perovskite Solar Cells Using Solution-Derived NiOx Hole Contacts. *ACS Nano* 10 (3), 3630–3636.
- Yoo, G.Y., Nurrosyid, N., Lee, S., Jeong, Y., Yoon, I., Kim, C., Kim, W., Jang, S.-Y., Do, Y.R., 2020. Newly Developed Broadband Antireflective Nanostructures by Coating a Low-Index MgF₂ Film onto a SiO₂ Moth-Eye Nanopattern. *ACS Appl. Mater. Interfaces* 12 (9), 10626–10636.
- Yoon, J., Sung, H., Lee, G., Cho, W., Ahn, N., Jung, H.S., Choi, M., 2017. Superflexible, high-efficiency perovskite solar cells utilizing graphene electrodes: towards future foldable power sources. *Energy Environ. Sci.* 10 (1), 337–345.
- Zhao, J., Zhao, L., Deng, Y., Xiao, X., Ni, Z., Xu, S., Huang, J., 2020. Perovskite-filled membranes for flexible and large-area direct-conversion X-ray detector arrays. *Nat. Photonics* 14 (10), 612–617.
- Zheng, L., Xuan, Y., 2021. Performance estimation of a V-shaped perovskite/silicon tandem device: A case study based on a bifacial heterojunction silicon cell. *Appl. Energy* 301, 117496.